BELLCOMM, INC.

TR-65-340-1

Solar Cosmic Ray Events

November 1, 1965

R. H. Hilberg

BELLCOMM, INC.

TABLE OF CONTENTS

BELLCOMM, INC.

ABSTRACT

15769

    Solar cosmic ray events are felt to present the greatest
hazard to the Apollo astronauts of all of the natural radiation
sources. This report describes the nature of the charged particle
fluxes in the vicinity of the earth in order to analyze the magni-
tude of the hazard.

    The temporal dependence, spectral shape, size and compo-
sition of the events of the 19th solar cycle peak (1956-1961) are
discussed. Best estimates for these properties are presented for
each event, and from these a dose-probability curve is calculated.
This is done using distribution functions to summarize the pro-
perties of the events.

    An effort is made to analyze the accuracy to which the
radiation environment has been measured. The detection systems
used are described with an estimate of the accuracy as well as the
overall advantages and disadvantages of each.

    Every effort should be made to reduce the uncertainties
of our knowledge of the next peak in solar activity. The ideal
program would include continuous monitoring outside of the magne-
tosphere of the particle flux, spectra, time dependence, and
composition.

Author

BELLCOMM, INC.

SOLAR COSMIC RAY EVENTS

I. Introduction

This report will present a description of the solar cosmic ray environment, with emphasis placed on developing an estimate of the uncertainty in the estimated hazard to the Apollo astronauts. Since our understanding of the environment is the result of various measuring devices, the merits and limitations of the instruments used in obtaining cosmic ray data will be analyzed. A useful method of applying the observed environment to describe the radiation hazard to the astronauts will be presented. The intention here is to emphasize basic aspects of the analysis of solar cosmic ray data rather than to present new or better data.

Solar cosmic ray events have been singled out from other sources of radiation because they are felt to present the greatest hazard to Apollo. The events of interest are those which produce high fluxes (of the order of 10^8 protons/cm^2 or more) with energies in the 1 Mev to 1 Bev range in the vicinity of the earth, lasting for several days. The characteristic of these events which is largely responsible for the hazard to Apollo is the fact that they occur randomly in time and cannot as yet be forecast in advance. The part of the energy spectrum of interest to the Apollo program is that between 30 Mev and 100 Mev. This is because protons with less than 30 Mev cannot penetrate the thinnest parts of the Command Module, while those with more than 100 Mev are much less numerous than those in the 30 to 100 Mev range. Protons with less than 30 Mev can penetrate the Lunar Excursion Module and the spacesuit, so they cannot be neglected for portions of the mission when some of the astronauts are outside the CM.

In short, the problems to be discussed in this report are:

(1) What do we know about the solar cosmic ray environment? How do we know it? How well do we know it?

(2) What do we want to know?

(3) How can the interaction of the cosmic ray environment
      with the Apollo astronauts be best analyzed?

2. Observations of Solar Cosmic Rays

          In this section the techniques used to measure solar
cosmic ray intensities, spectra, and composition as functions of
time will be described. The experimental uncertainties of the
obtained values will be estimated.

          There **was** no extended period of the 19th Solar Cycle
(1956-1961) during which complete coverage of the cosmic ray
environment was attained. All ground based observations required
detailed theoretical analysis to convert observed data to primary
cosmic ray fluxes in the energy range of interest. This analysis
was too complicated to give confidence in the results. In-flight
observations were not complete, with the times of peak flux occa-
sionally missed.

2.1 Polar Cap Absorption Measurements

          When energetic cosmic rays enter the atmosphere, they
lose energy by ionizing the air molecules. As the density of
ionization increases, the ability of radio waves to traverse the
medium decreases and the waves are absorbed.

          The three most successful systems which have been
developed to observe this phenomenon are the Riometer, the V.H.F.
ionospheric scatter network, and the F min system. The Relative
Ionospheric Opacity Meter (Riometer) measures the ionospheric
absorption of cosmic radio noise.[1] The V.H.F. ionospheric
scatter network transmits a radio wave from one station and
observes the wave after reflection from the ionosphere at a
second station about 1000 Km to 2000 Km away.[2] F min systems
measure the minimum frequency of radio waves that can be transmitted
vertically, with the echo from the ionosphere received on earth.
[2,3]

          The theory which relates the absorption of radio waves
by the ionosphere to the incident flux of cosmic rays is presented
by Leinbach.[1] The radio absorption depends on the density of
ionization-altitude profile, which in turn depends on the spectral
shape and intensity of the incident cosmic rays. Calculations
indicate that the observed absorption does not depend strongly on
the spectral shape.[4,5] Thus, only integral intensity values
above a cutoff energy can be expected.

The fact that most of the absorption is expected to occur at an altitude of 50-100 Km implies a minimum, atmospheric, cutoff energy of about 10 Mev. In addition, because of the earth's magnetic field, only particles above a particular cutoff rigidity can reach a given observer[11,14] with the value of the cutoff rigidity depending primarily on the magnetic latitude. Rigidity is defined by equation 3-4. The intensity of cosmic rays measured is thus the integral flux above the corresponding cutoff energy. Since the earth's magnetic field changes in magnetic storms, the value of the cutoff energy or the radio absorption may change during parts of the cosmic ray events.

Since the experimental accuracy is about the same for all PCA observations and the interpretive assumptions are similar, only Riometer data will be discussed here. The Riometer data is uncertain by about $\pm 20\%$ in the calculated absorption.[15] In addition to the purely experimental limitations, there is about a factor of 2 uncertainty in the interpretation of the data.[6]*

2.2 Neutron Monitors

Because of the dense atmosphere, very few cosmic rays reach the earth. However, many energetic (E>1 Bev) ones produce neutrons which can penetrate the atmosphere and be detected by earth based neutron monitors. Energetic solar cosmic rays and galactic cosmic rays both produce such neutrons, so that galactic cosmic rays produce a background counting rate which sets a lower limit on the solar cosmic ray fluxes observable with this type of monitor. Therefore, solar cosmic ray fluxes with few particles in the Bev range will not be seen.

Observations made at several stations located at different geomagnetic latitudes can yield integral fluxes above several energies. These integral fluxes can be combined to give information on the spectral shape of the particle fluxes in the Bev energy region.

The accuracy of the cosmic ray fluxes deduced from the neutron monitor is limited primarily by the considerations used in the interpretation. The yield depends to some extent on the spectral shape which is unknown unless spectral data from other

---

*This factor of 2 represents the expected error in the resulting flux value.

monitor stations or satellite observations are available. It
is estimated in the Solar Proton Manual[6] that cosmic ray
intensities are uncertain by up to a factor of two.

As indicated above, neutron monitors observe effects
produced by particles in the Bev energy range. Extrapolation
to the region of primary interest (30 Mev to 100 Mev) is
questionable, so that these measurements are not as valuable as
lower energy measurements. However, the monitoring is continuous
and the resulting checks on other measurements are helpful.

2.3 Primary Particle Detectors

Because of the earth's atmosphere, primary cosmic rays
can be detected only by in-flight detectors. The flight systems
used in the 19th solar cycle were balloons, rockets, and satel-
lites.

Balloons have the limitation that they cannot escape
the atmosphere completely, but the experiments use this fact to
advantage by using the residual atmosphere above the balloon as
an absorber and measuring integral fluxes. Spectral shapes can
be measured by observing integral fluxes during the ascent of the
balloon through the atmosphere.

Rockets containing detectors have been launched when
another system, such as the riometer, observed the presence of
solar cosmic rays. With such a flight system observers can com-
bine the advantage of continuous monitoring of the ground based
system with the increased data capabilities of in-flight measure-
ments.

Satellites offer the best coverage for monitoring in
the range of interest. The detectors can be selected from
considerations of the quantities to be measured with fewer re-
strictions set by the in-flight system.

Geiger counters detect only the passage of particles
through the Geiger tube and give no information on the energy or
specific energy loss. The specific energy loss of a particle is
defined as $-\frac{dE}{dx}$ (Mev-cm^2/gm) which is the energy deposited by a
particle per gram/cm^2 of material traversed. The range R of an
energetic proton is defined by:

$$R(E) = \int_E^O \frac{dE}{\left|\frac{dE}{dx}\right|}$$

where E is the initial energy of the particle. There is a 1:1
correspondence between the energy of a particle and its range
in a given material. Energy information can be obtained with
a Geiger tube by observing the flux of protons traversing a
given absorber, since all such protons have initial ranges
greater than the thickness of the absorber.

Ionization chambers count the total ionization of
particles passing through the counter. Usually an ionization
chamber measures "specific ionization". The fact that galactic
cosmic rays have lower specific ionization than solar cosmic
rays enables the ionization chamber to discriminate against
galactic cosmic rays better than the geiger counter. The combi-
nation of ionization chamber, geiger counter, and absorber enables
one to obtain information on spectrum and composition.

Scintillators with photomultiplier tubes and silicon
junction detectors have also been used to detect cosmic rays.
Both types measure the energy of the particle detected. Nuclear
emulsions have also been used. Emulsions give time integrated
energy and composition information but no information on temporal
dependence.

Except for the Geiger tubes, all of these detectors have
sufficient resolving power so that very little uncertainty is
introduced in measuring an integral energy spectrum by limitations
in detector resolution. Relatively high uncertainties are intro-
duced by geometrical and efficiency considerations. While the
efficiency of each of these detectors in detecting energetic pro-
tons and alpha particles is 100% under ideal conditions, statisti-
cal requirements combined with relatively low counting rates
necessitate non-ideal configurations. For example, rather than
use a thin scintillator on the surface of a photomultiplier with
good light collection, a large crystal with poor light collection
may be necessary. On such large detectors the efficiency is
difficult to calculate or measure. Complicated configurations of
absorbers and detectors combine with environmental conditions,
such as trapped radiation and the earth's magnetic field, to
restrict the accuracy of flux measurements. W. Webber estimates
an error of about $\pm 25\%$ for in-flight flux measurements.[3]

Table 1 summarizes the energy regions measured in the
19th solar cycle with the detection techniques used for each. It
is noted that satellite data extend back only to 1960. Since
balloons and rockets usually were launched after the arrival at
earth of cosmic rays, the data is more useful in giving spectral
shape than for time integrated fluxes.

Satellite data is superior to ground based and other in-flight data because it provides direct measurement of the particle fluxes throughout each event. However, better coverage could be obtained by means of a satellite which was outside of the magnetosphere a higher fraction of the time, ideally, all of the time.

3.   Characteristics of the 19th Solar Cycle Events

In this section the solar cosmic ray events of the 19th solar cycle will be described in some detail. The properties of the events will be discussed in an attempt to evaluate a standard format to which the majority of the events conform. Table 3 presents current best values for parameters used to describe the temporal dependence, the size, and the composition of each of the events of the 19th solar cycle. The significance of the parameters listed is described in this section. In order to make these quantities meaningful, the bulk of this section is given to a description of the phenomenology of the events as far as the near-earth region is concerned.

The forms in which the events are usually described will be presented and a table of the parameters applicable for each event (Table 3), will be included. It is not true that all events can best be described by the standard format, but it is desirable, from the point of view of analysis, to use a single representation.

3.1   Temporal Dependence

There are three characteristic times describing each cosmic ray event: the onset-delay time, the rise time, and the decay time. These quantities are shown in Figure 1. It should be noted that these quantities are different for each energy range considered.

It has become conventional to describe the temporal dependence of particle flux by exponential expressions:

$$J = J_p \exp \left(\frac{t-t_p}{t_R} \right) \qquad o < t \leq t_p \qquad (3-1)$$

$$J = J_p \exp \left(-\frac{t-t_p}{t_D} \right) \qquad t_p \leq t \qquad (3-2)$$

where J is the instantaneous particle flux rate, J_p is the peak particle flux rate, t_p is the time of peak flux, t_R is the rise time, and t_D is the decay time. To this approximation the time integrated particle flux is

$$N = \int_0^\infty J\, dt = J_p\, (t_R + t_D) \qquad (3\text{-}3)$$

Reference 6 presents the time dependence of most events. It can be seen that parts of most events can be described by such equations, but very few events can be described well during most of their duration by a single set of parameters. However, the values listed in Table 3 are useful in that they give a rough estimate of the duration of each event. While equations 3-1 and 3-2 are usually used to describe the temporal dependence of the flux intensity, they cannot be considered accurate representations but mere conveniences.

3.2 Spectral Shape

It has been found[7] that many cosmic ray events can best be described in terms of an exponential rigidity spectrum. A detailed discussion of this description, including examples, is found in Reference (7). The rigidity of a charged particle is defined as:

$$R = \frac{pc}{eZ} \qquad (3\text{-}4)$$

where p is the particle's momentum in Mev/c, c the velocity of light, e the absolute value of the charge of the electron in electrostatic units, and Z the atomic charge of the particle. Thus, the number of particles with rigidity greater than R is given by

$$N(>R) = N_o e^{-R/R_o} \qquad (3\text{-}5)$$

where R_o is the characteristic rigidity of the event and is defined by the above equation. The units of R are volts. A table relating energy to rigidity for protons, alpha particles, and electrons is given by McKee and Bohlin.[8]

Figure 2 gives the distribution of the observed values of characteristic rigidities for the events of the 19th solar cycle containing a total flux of 10^6 protons/cm^2 or more with energies greater than 30 Mev. $n(>R_o)$ represents the number of events having characteristic rigidity greater than R_o. The large uncertainties in the values prevent a unique choice of distribution functions from being chosen. Both the linear distribution

$$\int_{R_o}^{\infty} h(R_o)dR_o = \begin{cases} 1 & ; \ R_o < 40 \text{ Mv} \\ 1.3 - .0095 \ R_o & ; 40 \text{ Mv} < R_o \leq 145 \text{ Mv} \\ 0 & ; 145 \text{ Mv} < R_o \end{cases} \qquad (3\text{-}6)$$

and the exponential function

$$\int_{R_o}^{\infty} h(R_o)dR_o = e^{-R_o/52} \qquad (3\text{-}7)$$

fit the observed distribution to within experimental uncertainty. Both of these expressions fulfill the normalization requirement.

$$\int_{o}^{\infty} h(R_o)dR_o = 1 \qquad (3\text{-}8)$$

The advantage of the exponential rigidity spectrum description of an event is that a single parameter accurately describes the particle spectrum over wide ranges of rigidity or energy. This suggests that such a description may be basic to the acceleration and propagation process. However, the characteristic rigidity is not necessarily constant over an entire event. If the rigidity changes during an event, the time integrated spectrum may not be as accurately exponential as the instantaneous spectrum. Of the events considered in Reference 7, only about 30% had constant rigidity, with the characteristic rigidity

BELLCOMM, INC.   - 9 -

decreasing with time during the course of the other events.
Since the rigidity was fairly constant during the times of peak
flux, the time integrated spectrum was reasonably well described
by an exponential distribution in most cases.

3.3   Composition

        Data on the composition of solar cosmic rays is
limited, being available for only about 25% of the events of the
19th solar cycle. While the composition of solar cosmic rays
varies from one event to another, there is a tendency for protons
and alpha particles to be about equally abundant, with heavier

ions much less significant. Table 2 is taken from Schulte[9] and
gives relative fluxes of various positive ions based on data taken

from the September 3, November 12 and November 15, 1960 events.[10]
About 60% of the events observed contained proton/alpha particle
ratios consistent with the above assumption, while only a few
events were greatly at variance with it. For purposes of analysis
such a model is useful. The ratio of proton flux to alpha particle
flux is given in Table 3 for the events in which data is available.

3.4   Particle Fluxes

        The integral cosmic ray fluxes are usually presented in
terms of the total number of protons with rigidities greater than
R integrated over the time of the whole event, for R values of
137 Mv, 239 Mv, and 445 Mv (1 Mv = 10^6 v) corresponding to energies
of 10 Mev, 30 Mev and 100 Mev, respectively. In several cases,
when several events originated from the same spot on the sun and
were separated by only a few days, they were treated as a single
event in one curve in Figure 3. Such events which were close to
each other in both time of occurrence and in position on the sun
were considered to be a single solar event. The flux values are
the same as given in Table 3. The probability values were obtained
by assuming random time distribution during the 6 years of solar
maximum, 1956-1961.

        The event size distribution for the ungrouped events can
be described with fair accuracy by the expression:

$$\int_N^\infty g(N(>30))\, dN(>30) = \begin{cases} .0476 - .00511 \log_{10}\left[N(>30)\right]; N \leq 2\times10^9 \frac{protons}{cm^2} \\ 0 \qquad\qquad ; N > 2\times10^9 \frac{protons}{cm^2} \end{cases}$$

(3-9)

$$\int_{N(>30)}^{\infty} g(N'(>30))dN'(>30)$$ is the fraction of days in the 6 year

maximum of the 19th solar cycle in which an event of size $N(>30)$ or larger occurred.

The peak intensity, $J(>R)$, is given by

$$J(>R) = \frac{N(>R)}{t_R(R) + t_D(R)} \qquad (3\text{-}10)$$

to the extent that the exponential representation of the time dependence is correct.

Table 3 presents some significant parameters for the events of the 19th solar cycle. Values are taken from References 3 6 and 7 although most of them have been checked with calculations made from published data. The experimental uncertainties can be estimated from the values given in Table 1.

The first two columns give values for the onset plus rise time, expressed in hours, for protons above two energy levels. The next two columns contain decay times. Numbers given in parentheses are estimated values.

The next three columns contain total fluxes with energies above each of three values, integrated over the entire event. These fluxes are given in units of protons/cm^2.

The characteristic rigidities given are calculated from the equation

$$R_o = \frac{206}{\ln\left[\dfrac{N(>30\ Mev)}{N(>100\ Mev)}\right]} \qquad (3\text{-}11)$$

which results simply by assuming that the spectrum is accurately exponential in rigidity above 30 Mev. The data from 30 Mev to 100 Mev is used without regard to the flux above 10 Mev.

The errors assigned to the values in Figure 3 are based on error estimates summarized in Table 1. The rigidity values required two flux measurements (e.g., $N(>30\ Mev)$ and $N(>100\ Mev)$), and the error is propagated appropriately, using equation 3-11 as a definition.

The ratios of proton fluxes to alpha particle fluxes are based on fluxes per equal rigidity interval. It has been observed for some events that the same R_o describes α and proton spectra.[7,9] If this is generally true, then the ratio of proton to alpha particle fluxes should be independent of the rigidity range observed.

4. Applications

It is useful to use the empirical distribution functions presented in Section 3 in calculating a dose probability curve for the Command Module. The calculation which will be done is for a specific case, and the purpose of the calculation is to illustrate the use of the distribution functions.

The quantity to be evaluated is

$f(D)dD$ = the probability per day of being exposed to a dose between D and D+dD

The first assumption made is that the dose is a function of $N(>30)$ and the characteristic rigidity only, for a given shielding configuration:

$$D = D(N[>30], R_o) \qquad (4-1)$$

and that any one of these quantities can be expressed in terms of the other two.

$F(N[>30], R_o) \, dR_o dN[>30]$ represents the number of events with characteristic rigidities between R_o and $R_o + dR_o$ and flux between $N[>30]$ and $N[>30] + dN[>30]$. For convenience, the symbol N will be used to represent $N[>30]$ in the following:

$$f(D)dD = \int' F(N,R_o)dR_o dN \qquad (4-2)$$

The prime on the integration indicates that only values of N and R_o related by equation 4-1 are included in the summation.

The next simplifying assumption that will be made is that N is independent of R_o, so that

$$F(N,R_o) = g(N)h(R_o) \qquad (4-3)$$

The events of the 19th solar cycle are plotted as a function of N[> 30 Mev] and R_o in Figure 5. While the points do not seem purely random, there is no 1:1 relationship between N[> 30 Mev] and R_o, and the assumption of a random scatter should introduce only a small error in the results.

Substituting equation 4-3 into 4-2:

$$f(D)dD = \int' g(N) \ h(R_o) \ dR_o dN \qquad (4-4)$$

$$= \int g(N[D,R_o]) \ h(R_o) \ \frac{\partial(R_o,N)}{\partial(R_o,D)} \ dR_o \ dD$$

$$= \int g(N[D,R_o]) \ h(R_o) \ \frac{\partial N}{\partial D} \ dR_o \ dD \qquad (4-5)$$

or

$$f(D) = \int_0^\infty \frac{\partial N}{\partial D} \ g(N) \ h(R_o) \ dR_o \qquad (4-6)$$

$\frac{\partial(R_o N)}{\partial(R_o D)}$ is the Jacobian of the transformation from R_o,N coordinates to R_o, D coordinates.

It should be noted that g(N), f(D), and F(N,R_o) are defined as probabilities per day, while h(R_o) is normalized to unity.

A calculation by E. N. Shipley[12] indicated that the Command Module dose per proton or alpha particle depends on the characteristic rigidity in the manner shown in Figure 4. Since many solar cosmic ray events seem to have equal fluxes of protons and alpha particles per rigidity interval, this equality can be taken as universal for the purposes of the present analysis. For this case, Figure 4 indicates that the expression

$$D(N[>30 \ Mev],R_o) = 0.45 \times 10^{-9} \ N[>30 \ Mev] \ R_o \qquad (4-7)$$

empirically describes the dose given by an event of the size given by N and a spectral shape described by R_o. This expression is valid at the center of the capsule for this particle composition using the particular shielding described in Ref. 12. The simplicity of (4-7) is fortuitous, as is suggested by the three curves of Figure 4.

Equation (3-9) states that

$$\int_N^\infty g(N(>30)) \, d\, N(>30) = \begin{cases} .0476 - .00511 \, \log_{10}\left[N(>30)\right]; N \leq 2 \times 10^9 \, \dfrac{protons}{cm^2} \\ \\ 0; \qquad 2 \times 10^9 < N \qquad \dfrac{protons}{cm^2} \end{cases} \qquad (4\text{-}8)$$

which yields:

$$g(N(>30)) = \begin{cases} .00221/N \; ; \quad N \leq 2 \times 10^9 \qquad \dfrac{protons}{cm^2} \\ \\ 0 \quad ; \qquad 2 \times 10^9 \, \dfrac{protons}{cm^2} < N \end{cases} \qquad (4\text{-}9)$$

From equation (3-6):

$$\int_{R_o}^\infty h(R_o)dR_o = \begin{cases} 1 & ; \; R_o < 40 \; Mv \\ 1.3 - .0095 \, R_o; & 40 \leq R_o \leq 145 \; Mv \\ 0 & ; \; 145 < R_o \end{cases} \qquad (4\text{-}10)$$

which yields:

$$h(R_o) = \begin{cases} 0 & ; \; R_o < 40 \; Mv \\ .0095 \; ; & 40 \leq R_o \leq 145 \; Mv \\ 0 & ; \; 145 < R_o \end{cases} \qquad (4\text{-}11)$$

When equation (4-7) is solved for N, one has:

$$N = \frac{D}{.45 \times 10^{-9} R_o} \qquad (4\text{-}12)$$

Substituting equations 4-9, 4-11, and 4-12 into 4-6 and integrating, we have

$$f(D) = \begin{cases} \dfrac{2.2 \times 10^{-3}}{D} & ; D \leq 36 \text{ rad.} \\[2mm] \dfrac{2.1 \times 10^{-5}}{D} (145 - D/.9) & ; 36 \text{ rad} \leq D < 131 \text{ rad.} \\[2mm] 0 & ; D > 131 \text{ rad.} \end{cases} \quad (4\text{-}13)$$

$$\int_D^\infty f(D)dD = \begin{cases} .010 - .005 \log_{10}D & ; \quad D < 36 \text{ rad.} \\ .012 - .007 \log_{10}D + 2.3 \times 10^{-5}D & ; 36 \leq D \leq 131 \\ 0 & ; \quad 131 < D \end{cases} \quad (4\text{-}14)$$

This distribution function is shown in Figure 6 along with Shipley's calculated dose points.

An interesting aspect of the dependence of the dose distribution on $h(R_o)$ can be seen by considering

$$f(D) = \int_0^\infty \frac{\partial N(D,R_o)}{\partial D} \; g(N[D,R_o]) \; h(R_o)dR_o \quad (4\text{-}15)$$

In general this is a complicated function of $N(D,R_o)$ $g(N)$, and $h(R_o)$. For the reasonable case (see (4.9))

$$g(N) = \frac{\lambda}{N} ; 0 < N < \infty \quad (4\text{-}16)$$

we have:

$$f(D) = \int_0^\infty \frac{\partial N(D,R_o)}{\partial D} \; \frac{\lambda}{N(D,R_o)} \; h(R_o) \; dR_o \quad (4\text{-}17)$$

which depends on $N(D,R_o)$ and $h(R_o)$. If we now assume

$$N(D,R_o) = m(D)n(R_o) \quad (4\text{-}18)$$

$$f(D) = \int_0^\infty \frac{dm(D)}{dD} \; \frac{\lambda}{m(D)} \; h(R_o)dR_o$$

$$= \frac{\lambda}{m} \; \frac{dm(D)}{dD} \quad (4\text{-}19)$$

because of the normalization requirement of $h(R_o)$ (equation 3-8).
Thus, for the case where equations 4-16 and 4-18 hold, the dose
distribution is independent of the rigidity distribution, and a
single typical rigidity value can be assumed to apply to all
events in calculating a dose distribution. The particular rigidity
value chosen affects the normalization and, therefore, the
maximum possible dose, but does not affect the shape of the
distribution. The generality of this result is limited by the
finite range of validity of 4-6 in the real case, which results
in an overestimate of the dose probability in the regions of
these limits.

The analysis of the distribution of doses for the
events of the 19th solar cycle by the present method does not
introduce significant new information but is intended to demon-
strate the use of this approach. Dose is not a basic quantity,
especially when an arbitrary shield such as the command module
is introduced. A basic theory of cosmic ray events should be
able to reproduce the distribution functions.

While no events have been observed giving a dose
in the range of 200 rads, an extrapolation can reasonably
be made using above considerations. Such extrapolations
can be verified only by extensive additional data. How-
ever, extrapolations are often necessary, and the above method
may well give more reliable results than previous analyses.

There is no guarantee that the events of the 20th
solar cycle will be similar to those of the 19th. Therefore,
it is important that spectral, intensity, and composition
data be obtained as early in the 20th solar cycle as possible.
This would mean continuous monitoring, using all systems that
were used in the last solar cycle, as well as any improvements
now available.

5. Conclusions and Recommendations

While considerable effort has gone into experiments
measuring solar cosmic ray properties, the accuracy of the
results is still not as high as is needed for a reliable
picture of the overall phenomenon. The number of events
occurring in a given solar cycle is relatively small so that
statistics are poor, and direct measurements were made on a
regular basis only late in the cycle.

Another quantity affecting charged cosmic rays is
the earth's magnetic field. The problem of estimating the
equivalent free space acceptance solid angle of a detector
in low earth orbit is extremely complicated, even in times

of magnetic calm. Therefore, it should be helpful to make flux measurements outside of the earth's magnetosphere, on as continuous a basis as possible.

An ideal experimental program concerning the solar cosmic ray environment would include full time monitoring (outside of the magnetosphere) of particle flux, spectra, and time dependence of each type of particle present, and the relative abundances of each type. Such information would enable a more reliable environmental model to be developed.

1011-RHH-gdr   R. H. Hilberg

BELLCOMM, INC.

BIBLIOGRAPHY

(1) H. Leinbach, "Interpretations of the Time Variations of
     Polar Cap Absorption Associated with Solar Cosmic Ray
     Bombardments", Geophysical Institute of the University
     of Alaska, Scientific Report No. 3(May 1962).

(2) D. K. Bailey, "Polar Cap Absorption", Planetary Space
     Science 12 pp 495-541 (1964).

(3) W. R. Webber, "An Evaluation of the Radiation Hazard
     Due to Solar Particle Events", Boeing Co. Report D2-90469,
     (December 1963).

(4) R. R. Brown and R. A. Weir, "Ionospheric Effects of Solar
     Protons", Arkiv furGeofysik 3, pp 523-529, (1961).

(5) D. K. Bailey, "Abnormal Ionization in the Lower Ionosphere
     Associated with Cosmic Ray Flux Enhancements", Proceedings
     IRE, 47 (2), pp 255-266 (February 1959).

(6) F. McDonald, ed. "Solar Proton Manual", NASA TR R-169 (1963).

(7) Freier & Webber, JGR 68 (6), p 1605 (March 1963).

(8) McKee & Bohlin, SUI Report, SUI-63-22.

(9) H. J. Schulte, "Models for Space Environmental Hazards;
     Radiation", Bellcomm Report, Issue II, January 31, 1964.

(10) S. Biswas, et al, JGR 68, p 3109 (1962).

(11) M. S. Vallarta, Handbuch für Physik 46 (1), p 88 (1961).

(12) E. N. Shipley, Bellcomm Technical Memorandum, TM-64-1012-2
     (July 15, 1964).

(13) NASA Publication MDE 8020.008B SE015-001-1, p 39 (1965).

(14) J. J. Quenby & W. R. Webber; Phil. Mag. 4 p 90 (1959).

(15) H. Leinbach; Op. cit. p 61

(16) NASA Technical NOTE TN D-1061 and TN D-1139

(17) K. W. Ogilvie et al, J.G.R. 67 (3) p 929 (March, 1962).

(18) J. F. Steljies & H. Carmichael, J.G.R. 66 (5) p 1363 (May 1961).

(19) B. Maehlum et al, State University of Iowa Report - SUI 62-7 (1962).

(20) C. G. Little & H. Leinbach, Proc IRE 46 p 335 (Jan., 1958).

(21) P. Moyer, et al, P.R. 104, p 768 (1956).

(22) D. Reitz, NASA Reproduction N 63 - 19183 (1963).

(23) K. A. Anderson, et al, J.G.R. 64 (9), pp 1133-1147 Sept, 1959.

(24) J. R. Winkler & P. D. Bhanvar, J.G.R. 65 (9), pp 2637-2655 (1960).

(25) J. R. Winkler, et al, J.G.R. 66 (4) pp 995-1022 (1961).

(26) Anderson & Enemark, J.G.R. 65 (9) p 2657 (1960).

(27) McCracken & Palmeira, J.G.R. 65 (9), p 2673 (Sept, 1960).

(28) W. C. Lin, SUI-61-16 or W. C. Lin and J. A. Van Allen SUI 63-15.

(29) J. R. Winkler, et al, J.G.R. 66 (4) p 1023 (1961).

(30) K. G. McCracken, J.G.R. 67 (2) p 435 (1962).

(31) S. Biswas & P. S. Freier, J.G.R. 66 (4) p 1029 (1961).

(32) S. Biswas, et al J.G.R. 67 (1) p 13 (1962).

(33) J. R. Winkler, et al P.R.L. 6 (9) p 488 (May 1, 1961).

(34) L. R. Davis, et al P.R.L. 6 (9) p 492 (May 1, 1961).

(35) J. G. Roederer, et al P.R.L. 66 p 1603 (1961).

(36) Lockwood & Shea, J.G.R. 66 (10) p 3083 (1961).

BELLCOMM, INC.

APPENDIX

The "Natural Environment and Physical
Standards for the Apollo Program"
Solar Cosmic Ray Environment

The "Natural Environment and Physical Standards for
the Apollo Program" M-D E 8020.008B (SE-015-001-1), April 1965,
contains a model representing the expected solar cosmic ray
environment. The description includes some collective proper-
ties of the events and a specific, more detailed account of a
typical event. The model is presented as a basis for design and
engineering specifications.

The NEPSAP "model" represents a standard established
for the various contributors to the Apollo Program. It gives
a complete description of the spectra, intensity, composition,
and temporal dependence of solar cosmic ray events with which
radiation induced quantities can be calculated. The fact
that parts of the description have not been verified experi-
mentally has not been emphasized since it is not relevant to
the establishment of the standard. Similarly, estimates of
the accuracy of the model are not presented.

The NEPSAP model is derived from the same data that
was used in this report, so that the two descriptions are generally
consistent. However, since the variation of event parameters
from one event to another is considerable, the event described
in NEPSAP will be consistent with values observed for very
few individual events. For instance, the temporal dependence
displayed gives a t_R (> 30Mev) $\doteq$ 20 hours and t_R (> 100 Mev)
$\doteq$ 15 hours. These values are representative of about 30% of
the events. The expression relating peak flux to time inte-
grated flux (peak flux = 6×10^{-6} x time integrated flux) and
the time dependence curves require a decay time of the order
of one day, which is the average decay time of all events.
However, 50% of the events had decay times differing from this
by over eight hours.

As a standard, the description given in NEPSAP is an
adequate representation of the solar cosmic ray environment.
It is sufficiently complete that it allows extensive calculations
to be made of any of the radiation effects resulting from solar
cosmic ray events. It is sufficiently accurate that the results
of calculations can be relied on to the extent that a factor
of about 2 in the radiation exposure is unimportant.

FIGURE I   TIME DEPENDENCE OF PARTICLE FLUX

Number of Events with Rigidity Greater than R_0 $n(>R_0)$

Characteristic Rigidity R_0 (Mv)

$n(>R_0) = 90e^{-R_0/52}$

$n(>R_0) = 44.1 - .304R_0$
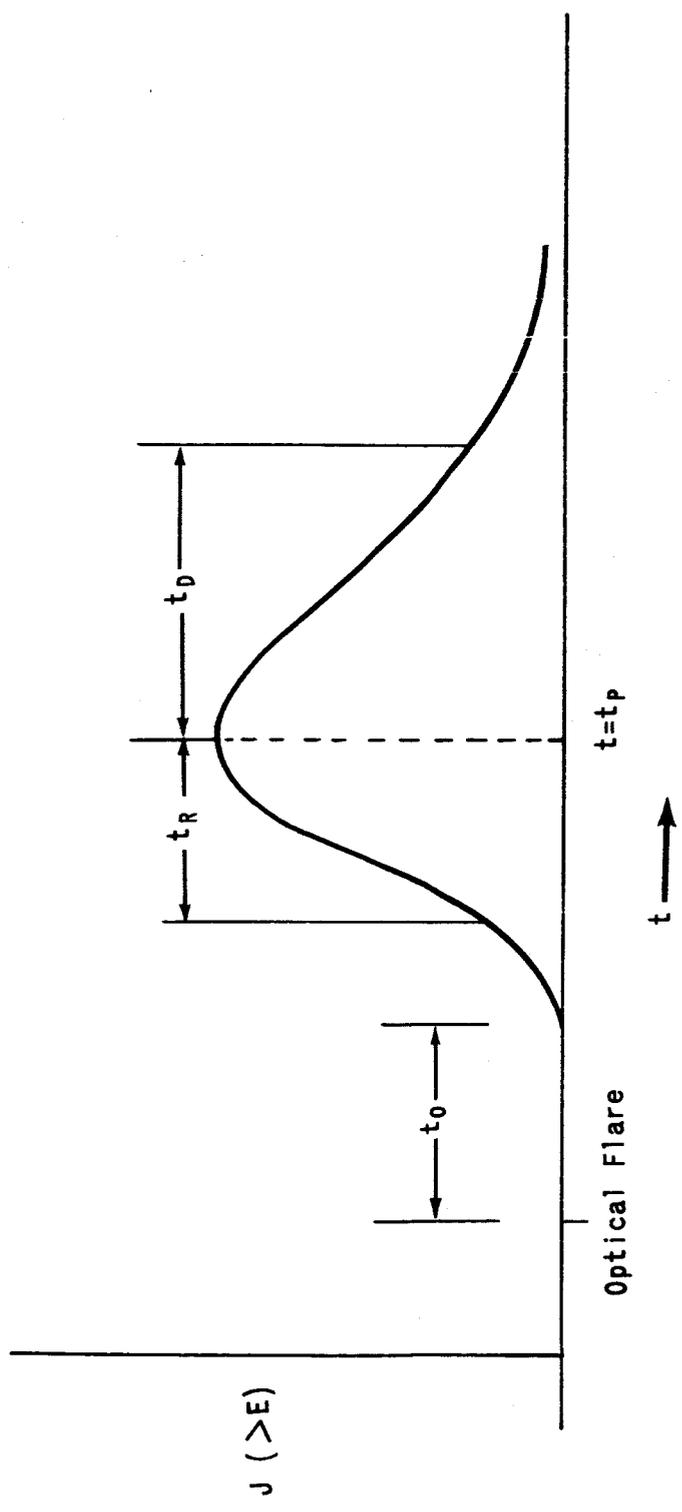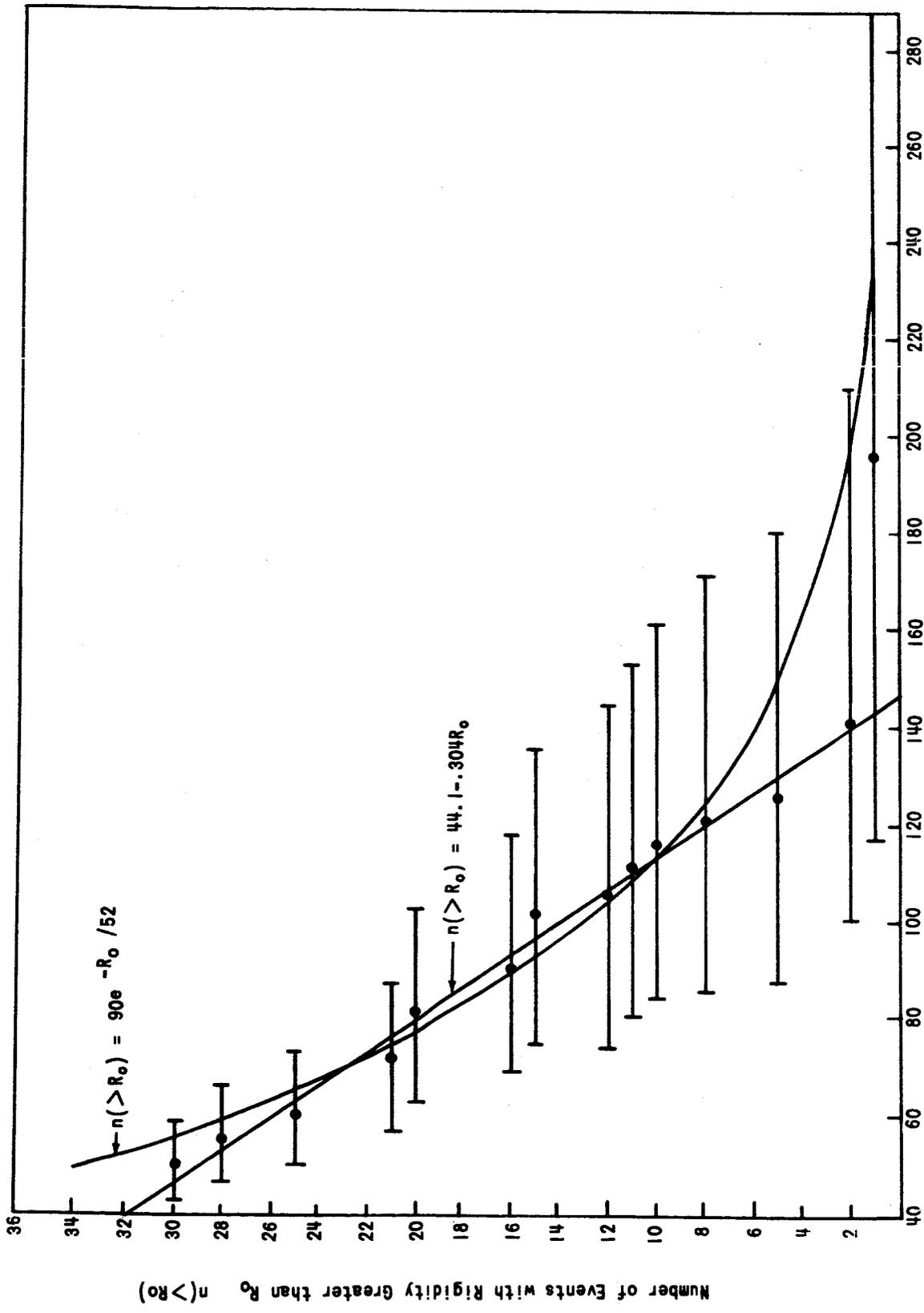
FIGURE 2   DISTRIBUTION OF CHARACTERISTIC RIGIDITY
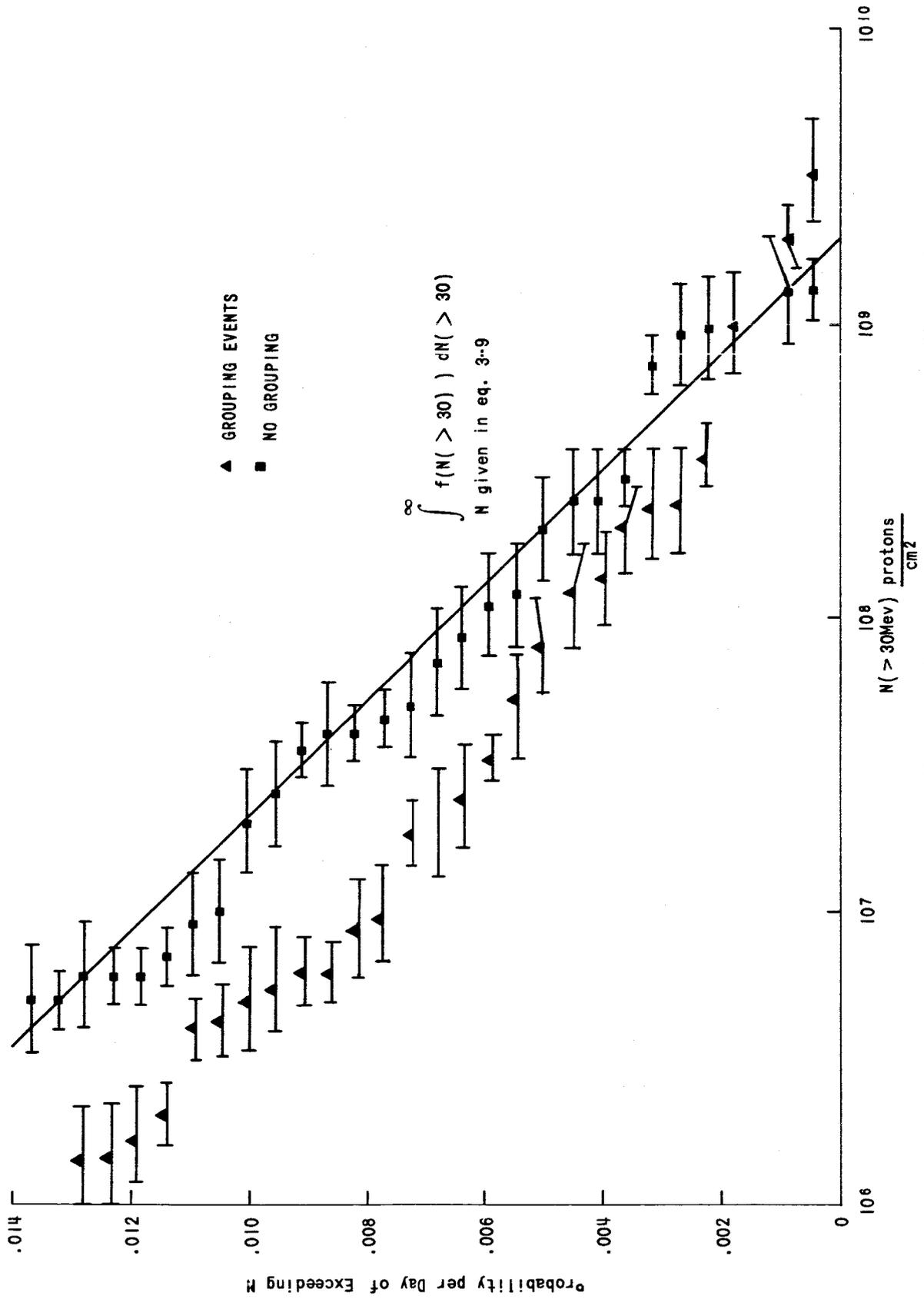
FIGURE 3   INTEGRAL FLUX DISTRIBUTION - PROBABILITY PER DAY OF EXCEEDING   N(> 30Mev)
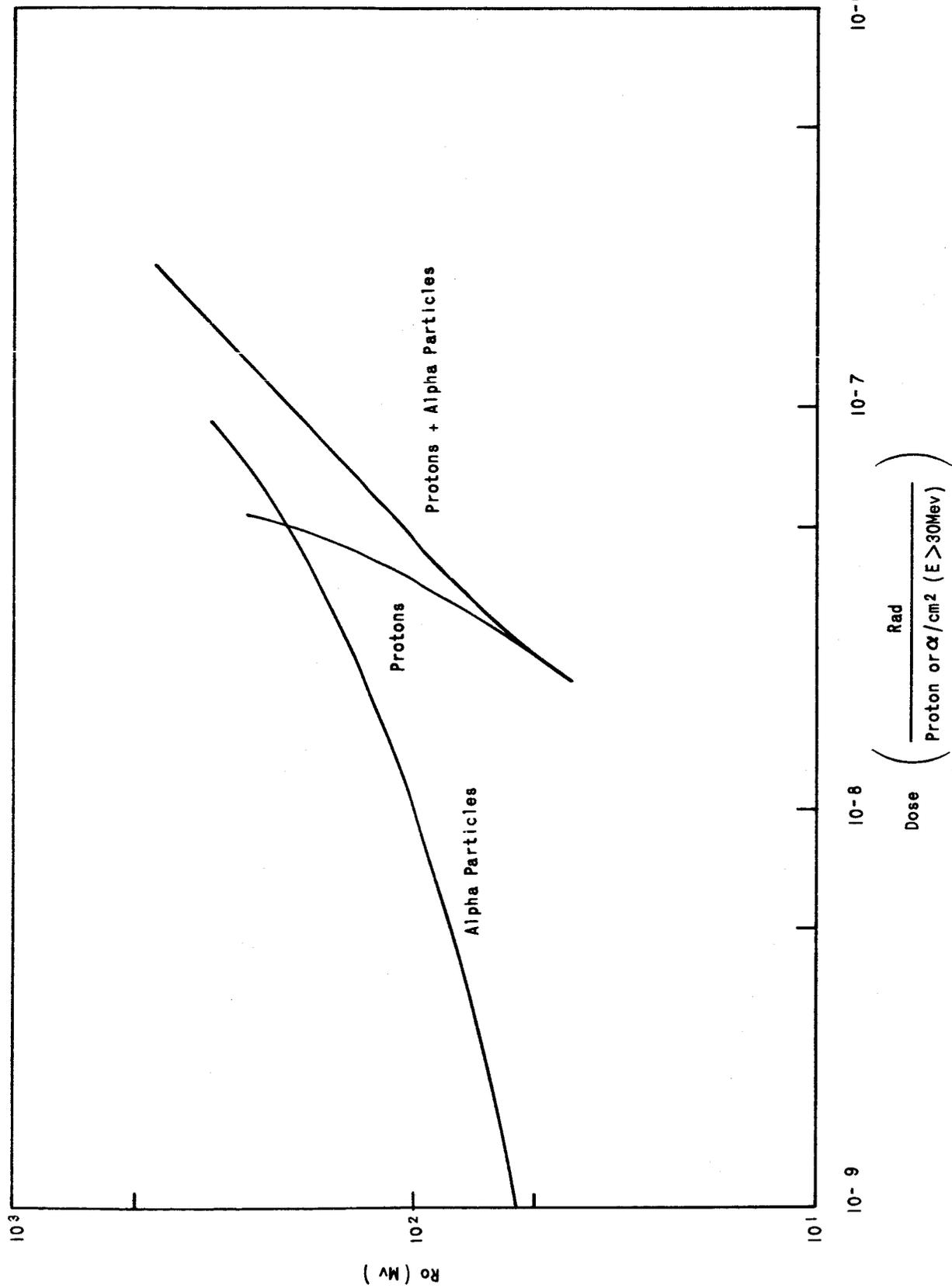
FIGURE 4   EFFICIENCY OF PRODUCING DOSE OF DIFFERENT PARTICLE SPECTRA
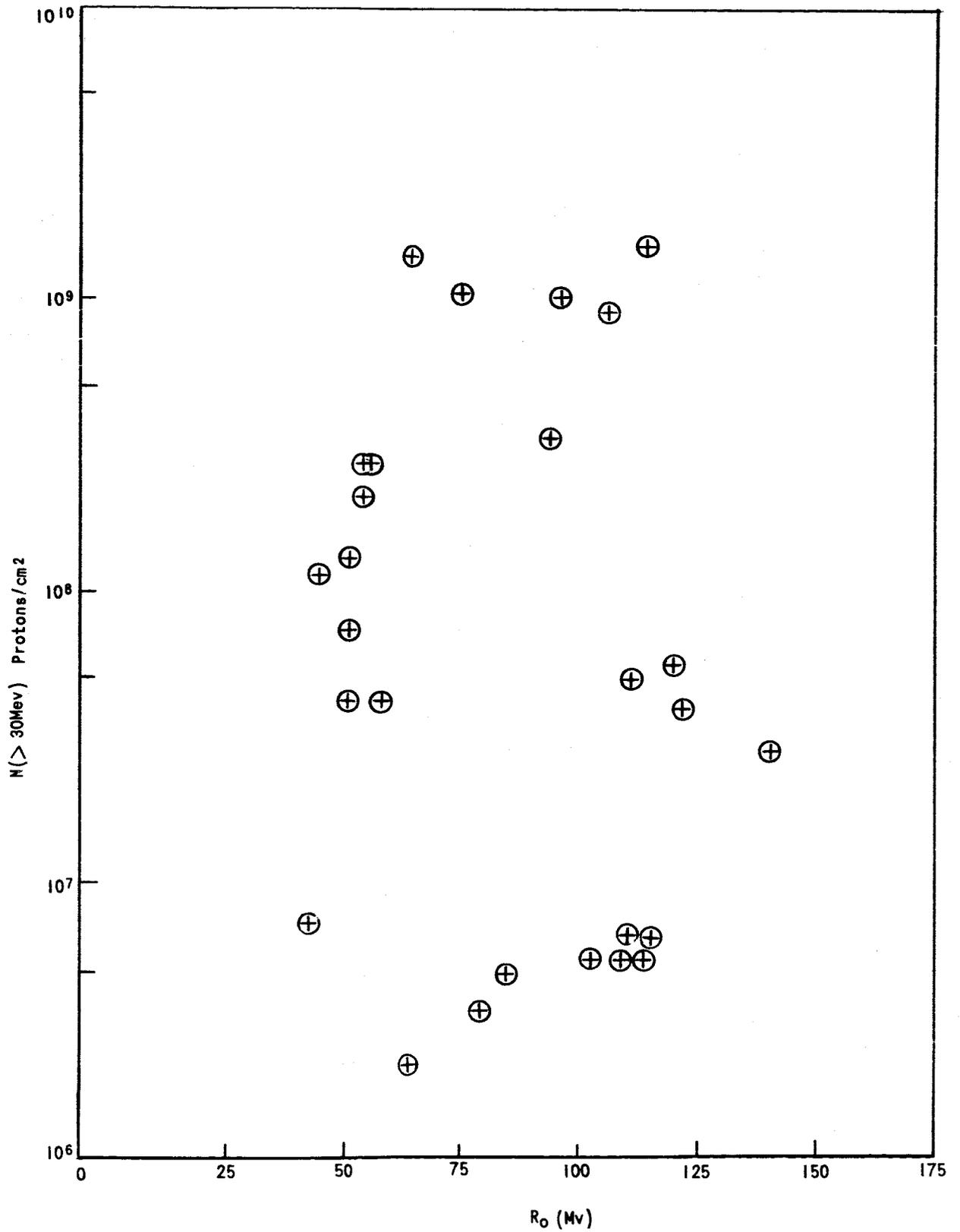
FIGURE 5   CORRELATIONS BETWEEN EVENT SIZE AND R_O
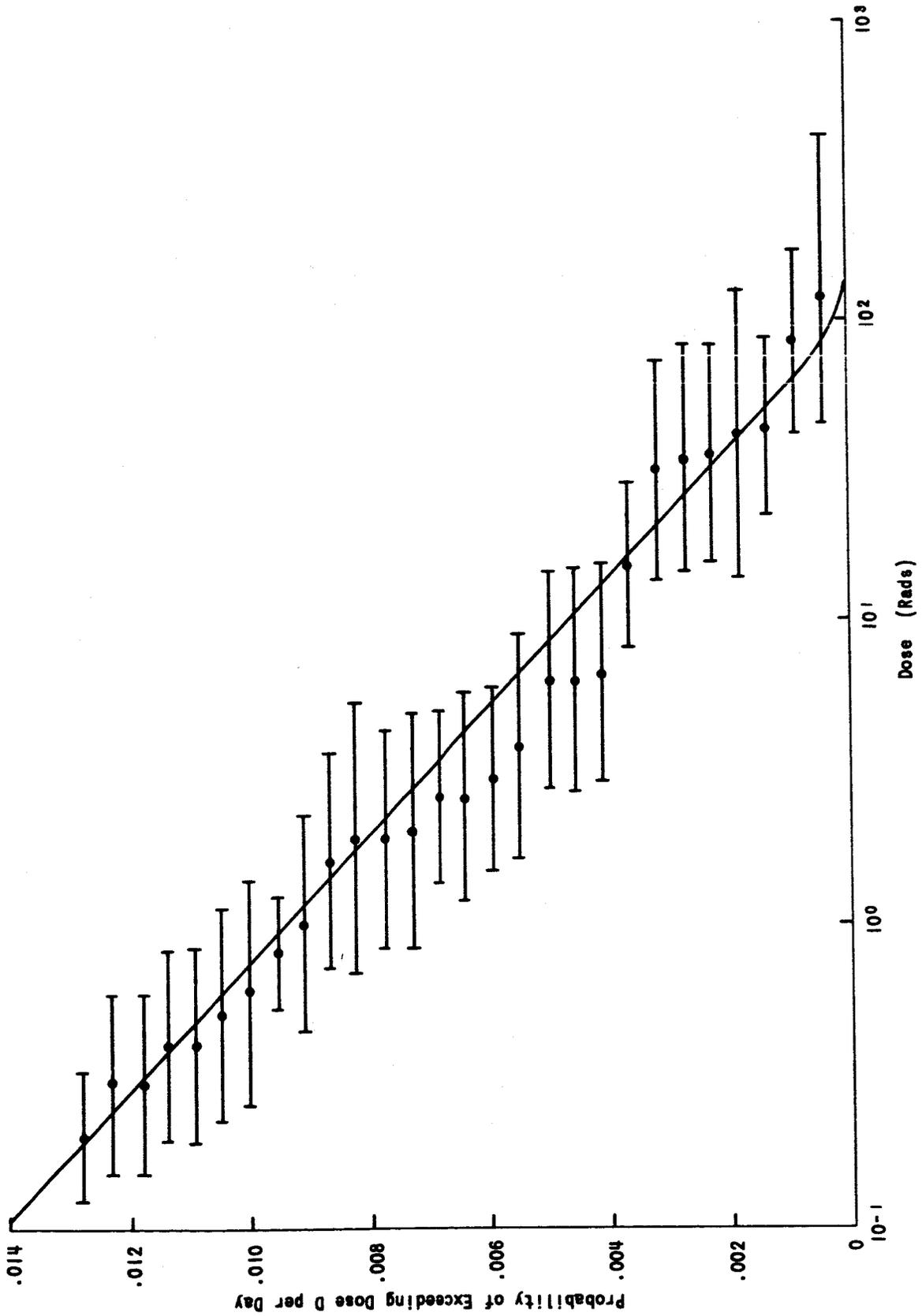
FIGURE 6   COMPARISON OF DOSE PROBABILITY CURVE PREDICTED FROM DISTRIBUTION FUNCTIONS
WITH DOSE ESTIMATES FROM INDIVIDUAL EVENTS

TABLE 1

COVERAGE OF SOLAR COSMIC RAYS

IN THE 19th SOLAR CYCLE

Detector	Integral Intensity				Spectral Shape (accuracy)	Composition	Time dependence	Event Coverage
	N(>10) (accuracy)	N(>30) (accuracy)	N(>100) (accuracy)	N(>1000) (accuracy)				
PCA	+100% − 50%				—	—	fair	Complete
Neutron Monitor	—		—	+100% − 50%	+100% − 50%	—	fair	Complete
Balloons & Rockets (i.e., G.T. Emulsions Scint. Junctions)	—		+25%	+25%	+50%	Some Coverage	incomplete	about 70% after 8/58
Satellites (i.e., G.T. Scint. Junctions)	—	+25%	—	—	+50%	—	fair	complete in 1960 + 1961

BELLCOMM, INC.

TABLE 2

Element	Relative Flux
Hydrogen	1
Helium	1
Beryllium and Boron	$<2 \times 10^{-4}$
Carbon	5×10^{-3}
Nitrogen	1×10^{-3}
Oxygen	9×10^{-3}
Fluorine	$<3 \times 10^{-4}$
Neon	1×10^{-3}
Sodium through Argon	1×10^{-3}

TABLE 2. – Relative fluxes of various elements in solar cosmic rays for equal rigidity intervals.

TABLE 3

Date	$t_R(>30$ MeV): Hours	$t_R(>100$ MeV): Hours	$t_D(>30$ MeV): Hours	$t_D(>100$ MeV): Hours	$N(>10$ MeV): Protons/cm^2	$N(>30$ MeV): Protons/cm^2	$N(>100$ MeV): Protons/cm^2	P_o (Mv)	Composition P/α (Proton to alpha ratio for a fixed energy)	Ref.
2/23/56	6	3	30	16	1.8 x 10^9	1.0 x 10^9	3.5 x 10^8	195		(2)(20)(21)(22)
8/31/56			(36)			2.5 x 10^7	6 x 10^6	144		(2)
1/20/57			(24)			2 x 10^8	7 x 10^6	61		(2)
7/3/57			(30)			2 x 10^7				(23)(2)
8/9/57			(18)			1.5 x 10^6	3 x 10^6	56		(2)
8/29/57			(60)			1.2 x 10^8				(23)(2)
9/21/57			(24)			1.5 x 10^6	1 x 10^7	127		(2)
10/20/57			(30)			5 x 10^7				(2)
11/4/57			(18)			9 x 10^6				
2/9/58			(18)			1 x 10^7				(2)
3/23/58			40	20	2 x 10^9	2.5 x 10^8	1 x 10^7	64	1.0 ± 0.5	(2)(1)
4/10/58						5 x 10^6	9 x 10^6			(2)(1)
7/7/58			32	16	1.8 x 10^9	2.5 x 10^8		62		(2)(1)
8/16/58	10		18		4 x 10^8	4 x 10^7	1.6 x 10^6	64		(2)(1)
8/22/58	10	3	20	8	8 x 10^8	7 x 10^7	1.8 x 10^6	56		(2)(1)(23)

TABLE 3
p. 2

Date	$t_R(>30\ \text{Mev})$: Hours	$t_R(>100\ \text{Mev})$: Hours	$t_D(>30\ \text{Mev})$: Hours	$t_D(>100\ \text{Mev})$: Hours	$N(>10\ \text{Mev})$: Protons/cm²	$N(>30\ \text{Mev})$: Protons/cm²	$N(>100\ \text{Mev})$: Protons/cm²	P_o (Mv)	Composition P/α (Proton to alpha ratio for a fixed energy)	Ref.
8/26/58	20		12		1.5×10^9	1.1×10^8	2.0×10^6	51		(2)(1)
9/22/58			(30)		9×10^7	6×10^6	1×10^5	50		(2)
5/10/59	30	10	22	14	5.5×10^9	9.6×10^8	8.5×10^7	84	1.0 ± 0.5	(2)(1)(24)(7)
6/13/59	16	(24)				8.5×10^7				
7/10/59	12	18	40	20	4.5×10^9	1.0×10^9	1.4×10^8	104	2.2 ± 0.5	(2)(1)(25)
7/14/59		12	18	12	7.5×10^9	1.3×10^9	1.0×10^8	80	1.0 ± 0.5	(2)(1)(25)
7/16/59		4	30	18	3.3×10^9	9.1×10^8	1.3×10^8	105	1.0 ± 0.5	(2)(1)(25)(26)(27)(7)
8/18/59		(24)				1.8×10^6				
1/11/60	6		30			4×10^5				(28)
4/1/60	2-3	<1	6	4	1.5×10^7	5.0×10^6	8.5×10^5	116		(2)(1)(28)
4/5/60	3		12			1.1×10^6				(2)(1)(28)
4/28/60	3	2	8	5	1.3×10^7	5.0×10^6	7×10^5	104		(2)(1)(28)
4/29/60						7×10^6				(2)(1)(28)
5/4/60	2-3	1	14	6	1.2×10^7	6×10^6	1.2×10^6	127	≥ 1	(2)(1)(28)(29)(30)(31)
5/6/60	3		24			4×10^6				(2)(1)(28)
5/13/60	3		15		1.5×10^7	4×10^6	4.5×10^5	94		(2)(1)(28)

TABLE 3
p. 3

Date	$t_R(>30 \text{ Mev})$: Hours	$t_R(>100 \text{ Mev})$: Hours	$t_D(>30 \text{ Mev})$: Hours	$t_D(>100 \text{ Mev})$: Hours	$N(>10 \text{ Mev})$: Protons/cm^2	$N(>30 \text{ Mev})$: Protons/cm^2	$N(>100 \text{ Mev})$: Protons/cm^2	$P_o(\text{Mv})$	Composition (Proton to alpha ratio for a fixed energy) p/α	Ref
6/1/60	2		20			4×10^5				(28)
8/12/60	10		50			6×10^5				(28)
9/3/60	12	6	32	26	9×10^7	3.5×10^7	7×10^6	127	~40	(2)(28)(32)(33)(34)(16)(7)
9/26/60					2×10^7	2.0×10^6	1.2×10^5	73		
11/12/60	10	8	18	14	4×10^9	1.3×10^9	2.5×10^8	124	1.0 ± 0.5	(2)(28)(35)(36)(16)(17)(30)(18)
11/15/60	8	4	16	10	2.5×10^9	7.2×10^8	1.2×10^8	114	2 ± 1	(2)(28)(36)(30)(18)(7)
11/20/60	2	1	10	5	1.4×10^8	4.5×10^7	8×10^6	118		(2)(28)
7/11/61	8-10	4	22-26	18	1.7×10^7	3×10^6	2.4×10^5	81		(19)
7/12/61	8-12	6	16-20	12	5×10^8	4×10^7	1×10^6	56		(2)(19)(7)
7/18/61	6-10	2-3	24	12	1×10^9	3×10^8	4×10^7	102	6 ± 1	(2)(19)(7)
7/20/61	4-6	1.5	6-8	3	1.5×10^7	5×10^6	9×10^5	120		(19)
9/28/61	1.5	1	12	8	5×10^7	6×10^6	1.1×10^6	121		(1)

BELLCOMM, INC.

DISTRIBUTION LIST

NASA Headquarters

R. J. Allenby - SM
P. E. Culbertson - MTL
J. H. Disher - ML
F. P. Dixon - MTY
W. B. Foster - SM
E. Z. Gray - MT
J. K. Holcomb - MAO
T. A. Keegan - MA-2
J. W. Keller - RV-1
G. A. Lemke - MAR
D. R. Lord - MTX
S. C. Phillips - MA
M. J. Raffensperger - MTE
A. Reetz, Jr. - RV-1
L. Reiffel - MA
M. Savage - MAT
A. W. Schardt - SG
M. L. Seccomb - MAP
W. B. Taylor - MLA
J. H. Turnock - MA-4
NASA Hq. Library - ATSS-10

Manned Spacecraft Center

W. A. Lee - PA
J. Modisette - ET32
D. E. Robbins - ET32
J. F. Shea - PA
W. E. Stoney, Jr. - ET

Marshall Space Flight Center

R. D. Shelton - R-RP-N

Bellcomm

G. A. Brill
F. C. Childs
R. E. Gradle
J. A. Hornbeck
B. T. Howard
C. A. Lovell
J. Z. Menard
C. R. Moster
I. D. Nehama
I. M. Ross
T. H. Thompson
R. L. Wagner
All members, Division 101
Department 1023
Central File
Library